Nonlinear Dyn (2016) 86:1057–1067
DOI 10.1007/s11071-016-2946-3

ORIGINAL PAPER

Nonlinear dynamics of an asymmetric rotor-bearing system with coupling faults of crack and rub-impact under oil-film forces

Ling Xiang · Xueyuan Gao · Aijun Hu

Received: 6 February 2016 / Accepted: 5 July 2016 / Published online: 12 July 2016

Abstract The parametric instability of a rotor-bearing system with coupling faults of crack and rub-impact under nonlinear oil-film force is studied in this paper. A model considering time-varying crack stiffness, rub-impact force and nonlinear oil-film force is put forward to analyze the complicated nonlinear behaviors of the rotor-bearing system. The numerical simulation focuses on the effects of crack depth and the stator stiffness on the onset of instability and nonlinear responses of the rotor-bearing system by using bifurcation diagrams, Poincaré maps, largest Lyapunov exponent and frequency spectrum. The multiple periodic, quasiperiodic and chaotic motions are observed in this study. The results indicate that crack depth and stator stiffness have influences on the vibration and instability of the rotor-bearing system with varied rotating speed. The motion of the system with coupling faults shows strong nonlinearity and instability in high speed region. Moreover, crack depth and stator stiffness interfere with the formation of oil whirl, thus, making the oil whirl appear later. There also exists interaction among coupling multiple faults. The research discloses the worthy energy exchange phenomenon of multi-fault system and is helpful for fault diagnosis and vibration control of real rotor-bearing systems.

L. Xiang (✉) · X. Gao · A. Hu
Department of Mechanical Engineering, North China Electric Power University, Baoding 071003, Hebei Province, China
e-mail: ncepuxl@163.com

Keywords Rotor-bearing system · Nonlinear dynamics · Crack · Rub-impact · Oil-film forces

1 Introduction

Rotating dynamic system has widely applied in duty industrial machineries. The stability of system is a very important issue for design, manufacturing and control of rotating machinery. The instability of bearing-rotor system will bring strong vibration and even disastrous accident of machinery. For decades, a lot of research efforts have been devoted to study the stability and nonlinear dynamic analysis of flexible rotor-bearing system. Crack and rub-impact are two important faults in rotating machines. The rub-impact usually results from excessive vibration caused by other faults in practical rotor systems, such as imbalance, rotor crack, and oil-film instability. The rotor-bearing model takes the nonlinear oil force into account, but the other fault such as rub impact force may be neglected. An ever-increasing pursuit of higher power and efficiency has lead to highly stressed condition of rotating machine elements. Rotor-bearing system is becoming more flexible and operating under tighter clearances and harsh environment. Under these circumstances, the rotor-bearing system is likely to develop more faults, e.g., crack, rub, whip. The faults of these machineries are becoming complicated, and the multiple or coupled faults often occur at the same time. When two faults happen at the same time, richer and more complex nonlinear behavior of

the rotor system will emerge. So the dynamic behaviors of the bearing-rotor should be studied considering crack and rub-impact under nonlinear oil-film forces.

The vibration dynamics of cracked rotor system have been intensively studied by many researchers. Dimarogonas [1] presented an extensive review of the literature on vibration of cracked shaft. A comprehensive survey of simple rotors with transverse crack has been presented by Gash [2]. Jun et al. [3] analyzed the vibration of a simple rotor with breathing crack. Sekhar and Prabhu [4] have analyzed the transient response of cracked rotor passing through critical speed and investigated the effects of crack depth, unbalance eccentricity with phase and acceleration. Sinou and Lees [5] studied the influences of cracks in rotating shafts. Chan and Lai [6] reported digital simulation of a rotating shaft with a transverse crack. Darpe et al. [7] studied dynamics of two crack rotor. They modeled one crack as breathing fatigue crack and other as open crack to simulate the rotor stiffness asymmetry. They also investigated the effect of bow on the nonlinear nature of the crack response [8]. Meng [9] has researched the dynamic response in the subcritical and supercritical speed ranges, and he used the cross-coupling stiffness terms to detect crack. George [10] has presented a new method to identify the crack depth and the location of a transverse surface crack by measuring the coupled response of rotating shafts. These works demonstrated that it is important to study the dynamic response of cracked rotor, but the continuous work is necessary to be developed, in which the analysis should be made taking into account the dynamic behavior of a rotating system with coupling faults under the rub-impact phenomenon, considering the influence of model parameters and other fault force.

The dynamics of rotor to stator contact dynamics have been investigated extensively in the past by many researches. Muszynska [11] reported a comprehensive literary survey on rub-related phenomena. In the nineties, a great deal of work treated the nonlinear analysis on rotor to stator contact dynamics. Studies on these rubbing phenomena revealed that the rotating system showed a rich class of nonlinear related dynamics such as sub- and super-synchronous responses, quasiperiodic responses and even chaotic motions. Chu and Zhang [12] studied the nonlinear vibration characteristics of a rub-impact Jeffcott rotor. They also found that when the rotating speed is increased, the grazing bifurcation, the quasiperiodic motion and chaotic motion occur in the process of the rub-impact. Goldman and Muszynska [13] presented that the chaotic motion in a nonlinear study is more likely to occur if a proper impact model is employed. Issam [14] used numerical analysis and evolutionary algorithms to analyze the nonlinear dynamics of a rotor with rub-impact. Liu et al. [15] analyzed dynamic characteristics of a disk–drum–shaft rotor system with rub-impact. Lahriri [16] conducted the theoretical modeling, analysis and validation of the shaft motion and dynamic forces during rotor–stator contact.

Of the existing work, some works have thrown light to nonlinear coupled or interaction dynamics considering multi-fault forces. The research [17] performed a dynamic analysis of the rub-impact rotor supported by two couple stress fluid film journal bearings, and the strong nonlinear couple stress fluid film force and nonlinear rub-impact force are presented and coupled together. Shen et al. [18] presented experimental and numerical analysis of nonlinear dynamics of system considering rub-impact and oil-film forces. Wan et al. [19] used harmonic wavelet transform to analyze the vibration characteristics of cracked rotor sliding bearing system with rotor–stator rubbing. Ren et al. [20] applied multi-degrees of freedom system to study dynamic characteristics of rotor-bearing system with coupling faults of rub-impact and crack. The works [19,20] have focused on the interaction of crack and rub-impact in rotor-bearing system, but the detailed research should be carried out on nonlinear dynamics of a rotor-bearing system with coupling faults of crack and rub-impact under nonlinear oil-film force. All these researches have helped the identification of state for rotor-bearing system. But the coupling dynamics of crack and rub-impact under nonlinear oil-film force is the keystone of this paper. The orbits of shaft, Poincare maps, frequency spectrum and bifurcation diagrams, etc., are constructed to analyze the dynamic characteristic of rotor-bearing system. Numerous results reveal a nonlinear dynamic process including periodic, quasiperiodic and multi-periodic.

The remainder of this paper is organized as follows: Sect. 2 describes the mathematical model of the rotor-bearing system with coupling fault of crack and rub-impact under nonlinear oil-film force. Section 3 presents the numerical analysis results which include effects of crack and rub-impact on the dynamics of the rotor-bearing system. Finally, Sect. 4 presents some brief conclusions.

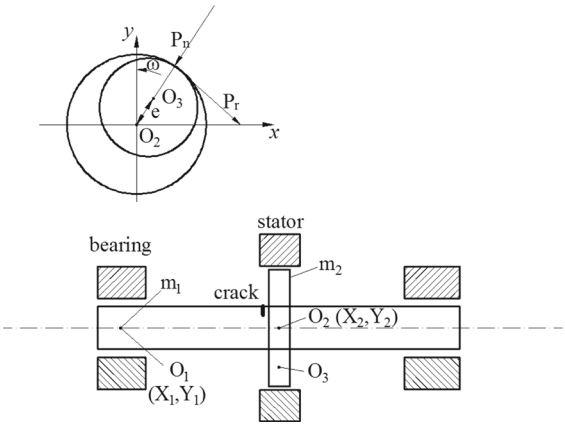

Fig. 1 Rotor-bearing system with coupling fault of crack and rub-impact

2 Mathematical model

As shown in Fig. 1, the model consists of one disk and a massless shaft supported by two symmetrical oil-film journal bearings. The oil-film journal bearing has a lumped mass m_1 at its geometric center O_1, while the disk at the center of the shaft takes a lumped mass m_2 at its geometric center O_2. O_3 is the centroid of the disk. There is a transverse bow crack near the disk. The impact of shear deformation, torsional vibration and gyroscopic couple is all neglected for highlighting the effect of oil-film force.

Where x_1 and y_1 are the radial displacements of the left shaft neck, and x_2 and y_2 are the radial displacements of the disk. The equations of motion for the cracked rotor-bearing system based on rotor dynamics theory can be written as

$$\begin{cases} m_1\ddot{x}_1 + c_1\dot{x}_1 - \frac{1}{2}k_{xx}(x_1 - x_2) - \frac{1}{2}k_{xy}(y_1 - y_2) \\ \quad = F_x \\ m_1\ddot{y}_1 + c_1\dot{y}_1 - \frac{1}{2}k_{yx}(x_1 - x_2) - \frac{1}{2}k_{yy}(y_1 - y_2) \\ \quad = F_y - m_1 g \\ m_2\ddot{x}_2 + c_2\dot{x}_2 + k_{xx}(x_1 - x_2) + k_{xy}(y_1 - y_2) \\ \quad = m_2 e\omega^2 \cos(\omega t - \beta) + P_x \\ m_2\ddot{y}_2 + c_2\dot{y}_2 + k_{yx}(x_1 - x_2) + k_{yy}(y_1 - y_2) \\ \quad = m_2 e\omega^2 \sin(\omega t - \beta) + P_y - m_2 g \end{cases} \tag{1}$$

where F_x, and F_y are the nonlinear oil-film forces, P_x and P_y are the rub-impact forces, $c_i (i = 1, 2)$ is the structure damping, and $k_{ij}(i, j = x, y)$ is the shaft stiffness considering crack.

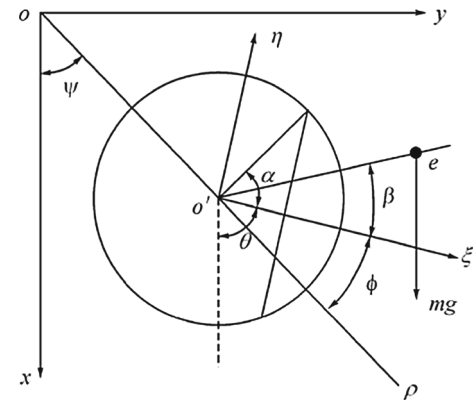

Fig. 2 Schematic diagram of switching crack model

2.1 Stiffness of the crack shaft

Figure 2 shows the cross section of the crack in the rotating shaft. The coordinate system $\xi o'\eta$ fixes on the disk and rotates with the disk. The direction of crack propagation is $o'\xi$, while $o'\eta$ is the vertical direction of crack propagation. k_0 is the stiffness of a non-crack shaft. e is the eccentricity. β is the angle between the direction of crack and the direction of unbalance. The stiffness matrix of the rotating shaft with the breathing crack can be expressed as

$$[K] = \begin{bmatrix} k_{xx} & k_{xy} \\ k_{yx} & k_{yy} \end{bmatrix} = \begin{bmatrix} k_0 & k_0 \\ 0 & 0 \end{bmatrix} - f(\phi) \times \begin{bmatrix} \Delta k_\xi \cos^2\varphi + \Delta k_\eta \sin^2\varphi & (\Delta k_\xi - \Delta k_\eta)\sin\varphi\cos\varphi \\ (\Delta k_\xi - \Delta k_\eta)\sin\varphi\cos\varphi & \Delta k_\xi \sin^2\varphi + \Delta k_\eta \cos^2\varphi \end{bmatrix} \tag{2}$$

$$f(\phi) = [(1 + \cos\phi)/2]^A \tag{3}$$

where $\varphi = \theta + \beta$, $A = a/R$. Δk_s $(s = \xi, \eta)$ is the change of the shaft stiffness caused by crack in ξ and η directions, and A is the nondimensional crack depth.

2.2 Rub-impact forces

It is assumed that the rub-impact occurs with a Hertz contact and a Coulomb friction. Then, when rub-impact occurs, two forces can be integrated for rub-impact force as shown in Fig. 1. One is called striking force P_n which is caused by the contact of the rotor against stator. It can be represented by using linear elastic deformation theory. Another is frictional force P_r, which is brought up by Coulomb law.

$$P_n = (r-\delta)\, k_c \,(r \geq \delta)$$
$$P_r = f \cdot P_n \tag{4}$$

where δ is the initial clearance between rotor and stator. r is the displacement of shaft center in radial direction and $r = \sqrt{x^2 + y^2}$.

The equations of rub-impact forces in x and y direction are formulated as follows:

$$\begin{bmatrix} P_x \\ P_y \end{bmatrix} = -\frac{(r-\delta)k_c}{r}\begin{bmatrix} 1 & -f \\ f & 1 \end{bmatrix}\begin{bmatrix} x \\ y \end{bmatrix}, \quad (r \geq \delta)$$
$$P_x = P_y = 0, \quad (r < \delta) \tag{5}$$

2.3 Model of oil-film forces

In this paper, the oil-film force generated by the sliding bearing is highly nonlinear, and the classical Capone circle bearing theory is applied in the theoretical analysis. The Reynolds equation can be modified and performed as [21] in Eq. (6). Integrating the Reynolds Eq. (6), the distribution of oil-film pressure is given as in Eq. (7). The nondimensional oil-film force components $\overline{fx}$ and $\overline{fy}$ can be written as in Eq. (8).

$$\left(\frac{R}{L}\right)^2 \frac{\partial}{\partial Z}\left(h^3 \frac{\partial p}{\partial Z}\right) = x\sin\theta - y\cos\theta$$
$$-2(x'\cos\theta + y'\sin\theta) \tag{6}$$
$$p = \frac{1}{2}\left(\frac{L}{D}\right)^2 \frac{(x-2y')\sin\theta - (y+2x')\cos\theta}{(1 - x\cos\theta - y\sin\theta)^3} \tag{7}$$
$$\begin{cases} f_X = \sigma \bar{f}_x; \\ f_Y = \sigma \bar{f}_Y \end{cases}$$
$$\sigma = \mu\omega RL\left(\frac{R}{c}\right)^2\left(\frac{L}{2R}\right)^2$$
$$\begin{bmatrix} \bar{f}_x \\ \bar{f}_y \end{bmatrix} = -\frac{\left[(x-2\dot{y})^2 + (x+2\dot{x})^2\right]^{1/2}}{1-x^2-y^2}$$
$$\times \begin{bmatrix} 3xV(x,y,\alpha) - \sin\alpha G(x,y,\alpha) - 2\cos\alpha S(x,y,\alpha) \\ 3xV(x,y,\alpha) + \cos\alpha G(x,y,\alpha) - 2\sin\alpha S(x,y,\alpha) \end{bmatrix} \tag{8}$$

where R is the radius of the bearing, c represents the bearing radial clearance, μ indicates the lubricating oil viscosity described, and L expresses the length of bearing.

The nondimensional parameters of the system are introduced as below

$$\alpha = \arctan\frac{y+2\dot{x}}{x-2\dot{y}} - \frac{\pi}{2}\sin\left(\frac{y+2\dot{x}}{x-2\dot{y}}\right)$$
$$-\frac{\pi}{2}\sin(y+2\dot{x})$$
$$V(x,y,\alpha) = \frac{2 + (y\cos\alpha - x\sin\alpha)\, G(x,y,\alpha)}{1-x^2-y^2}$$
$$G(x,y,\alpha) = \frac{2}{(1-x^2-y^2)^{1/2}}$$
$$\left[\frac{\pi}{2} + \arctan\frac{y\cos\alpha - x\sin\alpha}{1-x^2-y^2}\right]$$
$$S(x,y,\alpha) = \frac{x\cos\alpha + y\sin\alpha}{1-(x\cos\alpha + y\sin\alpha)^2} \tag{9}$$

The dynamics equations of the rotor-bearing system are given in Eq. (1), which have considered the influences of crack stiffness [Eqs. (2), (3)], rub-impact forces [Eq. (5)] and oil-film forces [Eq. (8)]. Nondimensional transformations of the system are given as

$$\bar{x}_1 = x_1/c, \quad \bar{y}_1 = y_1/c, \quad \bar{x}_2 = x_2/c, \quad \bar{y}_2 = y_2/c, \quad \tau = \omega t,$$
$$\xi_1 = \frac{c_1}{m_1\omega}, \quad \xi_2 = \frac{c_2}{m_2\omega}, \quad \eta_1 = \frac{k_0}{m_1\omega^2}, \quad \eta_2 = \frac{k_0}{m_2\omega^2}, \quad \bar{e} = \frac{e}{c},$$
$$G_0 = \frac{g}{c\omega^2}, \quad M = \frac{\sigma}{cm_1\omega^2}, \quad \gamma = \frac{\Delta k_\xi - \Delta k_\eta}{\Delta k_\xi}, \quad \Delta\bar{k}_\xi = \frac{\Delta k_\xi}{k_0},$$
$$\lambda_1 = (1-\gamma\sin^2\tau)(\bar{x}_1 - \bar{x}_2) + \gamma\sin\tau\cos\tau(\bar{y}_1 - \bar{y}_2),$$
$$\lambda_2 = \gamma\sin\tau\cos\tau(\bar{x}_1 - \bar{x}_2) + (1-\gamma\sin^2\tau)(\bar{y}_1 - \bar{y}_2)$$

Then, the nondimensional dynamics equation can be expressed as

$$\begin{cases} \ddot{\bar{x}}_1 = -\xi_1\dot{\bar{x}}_1 + \frac{1}{2}\eta_1(x_1 - x_2) - \frac{1}{2}f(\phi)\,\eta_1\Delta\bar{k}_\xi \\ \quad \times\lambda_1 + f_x \cdot M \\ \ddot{\bar{y}}_1 = -\xi_1\dot{\bar{y}}_1 + \frac{1}{2}\eta_1(y_1 - y_2) - \frac{1}{2}f(\phi)\,\eta_1\Delta\bar{k}_\xi \\ \quad \times\lambda_2 + f_y \cdot M - G_0 \\ \ddot{\bar{x}}_2 = -\xi_2\dot{\bar{x}}_2 - \eta_2(x_1 - x_2) + f(\phi)\,\eta_2\Delta\bar{k}_\xi \\ \quad \times\lambda_1 + e\cos(\tau - \beta) + P_x \\ \ddot{\bar{y}}_2 = -\xi_2\dot{\bar{x}}_2 - \eta_2(y_1 - y_2) + f(\phi)\,\eta_2\Delta\bar{k}_\xi \\ \quad \times\lambda_2 + e\sin(\tau - \beta) + P_y - G_0 \end{cases} \tag{10}$$

3 Nonlinear dynamic analysis

The numerical solution of Eq. (10) is performed by using fourth-order Runge–Kutta method. The results of the first 300 cycles are neglected to eliminate transient response. The time step for direct numerical integration is specified as $\pi/100$. The simulated model parameters of rotor-bearing system are given in Table 1. Bifurcation diagrams, time series, axis orbits, frequency spec-

Table 1 The simulated model parameters of rotor-bearing system

Parameters	Values
m_1, m_2 (kg)	4, 32
k_0 (N m^{-1})	2.5×10^7
f	0.1
R, L, c (mm)	25, 12, 0.11
μ (Pa s)	0.018
c_1, c_2 (N s m^{-1})	1050, 2100
e (mm)	0.05

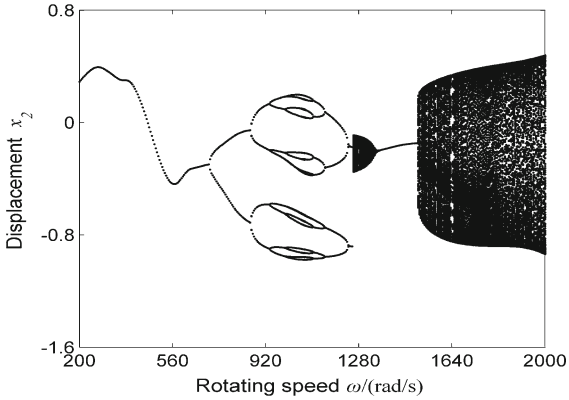

Fig. 3 Bifurcation diagram at $A = 0, k_c = 3.5 \times 10^6$ N m^{-1}

tra and Poincare maps are acquired by numerical integration. The largest Lyapunov exponent (LLE) can provide a quantitative analysis of motion state of the system, which is obtained unsuccessfully from neither the shaft orbit nor the frequency spectra of the rotor response.

3.1 Effect of rotational speed to the system

The bifurcation diagram of rotor-bearing system is shown in Fig. 3 with ω as control parameter. All the parameters are taken from Table 1. The largest Lyapunov exponent of rotor-bearing system is shown in Fig. 4. The rotor-bearing system is found to display a rich diversity of responses when $A = 0$ and $k_c = 3.5 \times 10^6$ N m^{-1}. There exist three motions which are the stable period-one (P1) motion, multiple periodic and quasiperiodic motions at $\omega = [200{-}2000]$ rad/s. The dynamic motion of the rotor system is synchronous with P1 before $\omega = 700$ rad/s. Then, it takes the

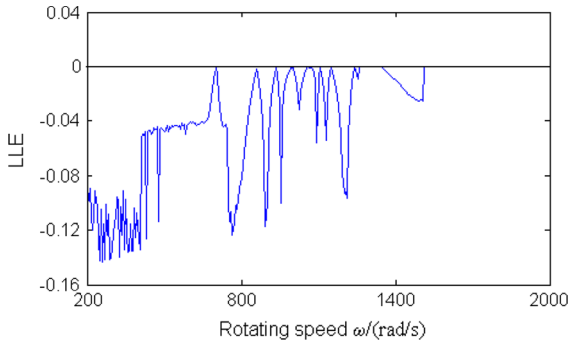

Fig. 4 Largest Lyapunov exponent at $A = 0, k_c = 3.5 \times 10^6$ N m^{-1}

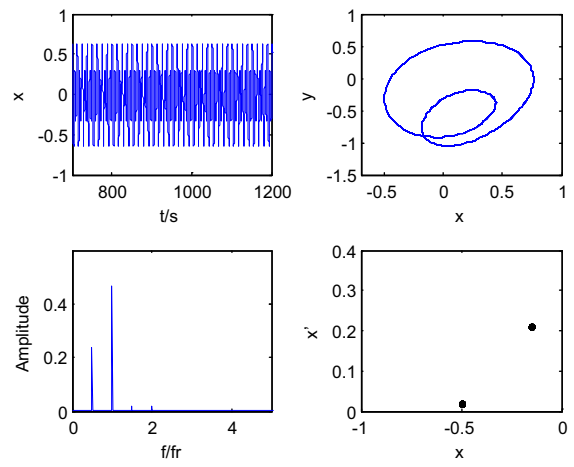

Fig. 5 Time series, axis orbit, frequency spectra and Poincare map at $\omega = 705$ rad/s

general form {P2 → P4 → P8 → P16 → P8 → P4 → P2} as the rotating speed is varied between the values [700 → 1225] rad/s. The corresponding value of LLE from Fig. 4 is zero at the bifurcation point from Fig. 3. It can be seen that the Poincare map has two isolated points in Fig. 3, so the axis orbit has two oval and the frequency spectra has two discrete frequency components in Fig. 5. The system is in a state of P2 motion, where the oil whirl and rub-impact exist at the same time. When $\omega = 1050$ rad/s, the axis orbit of the classic oil whirl has turned up in Fig. 6. Multiple frequency components exist in the frequency spectra, and the half-frequency amplitude almost equals the amplitude of fundamental frequency. There are 16 phase points on the Poincare map. Therefore, the oil whirl and rub-impact get stronger. As rotating speed increases, transient quasiperiodic motion happens at

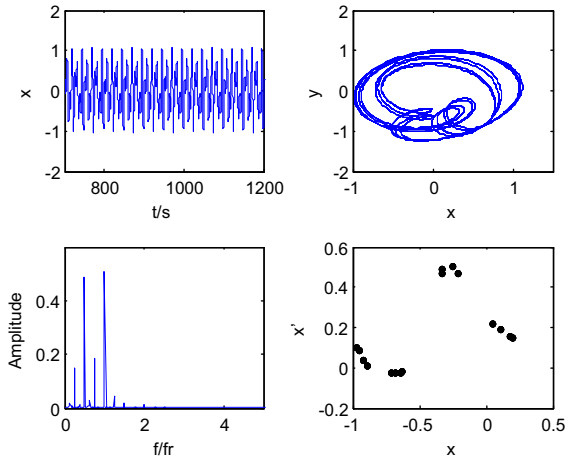

Fig. 6 Time series, axis orbit, frequency spectra and Poincare map at $\omega = 1050\,\text{rad/s}$

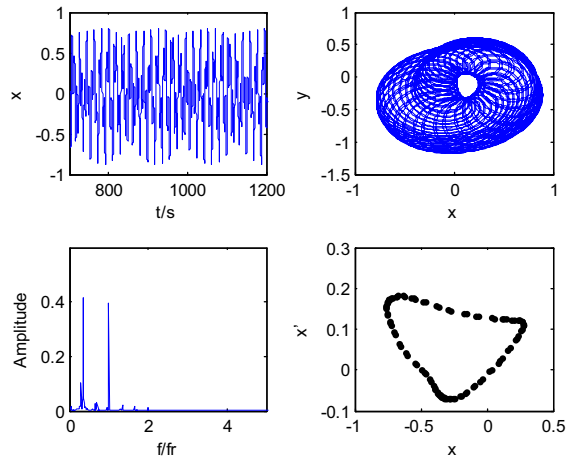

Fig. 7 Time series, axis orbit, frequency spectra and Poincare map at $\omega = 1550\,\text{rad/s}$

$\omega = [1255-1360]\,\text{rad/s}$, and the LLE in Fig. 4 is equal to zero. Then the system reenter into the P1 motion region, thus, returning to a relatively stable state. When $\omega = 1505\,\text{rad/s}$, the system goes into a long-term quasiperiodic motion after Hopf bifurcation. Distinct "beat" signals appear in time series in Fig. 7. The amplitude of oil whip frequency is considerably greater than that of fundamental frequency. A closed loop emerges on the Poincare map. It also can be concluded that the system is in quasiperiod motion. Here the oil whirl becomes into oil-whip, and rub-impact is still severe.

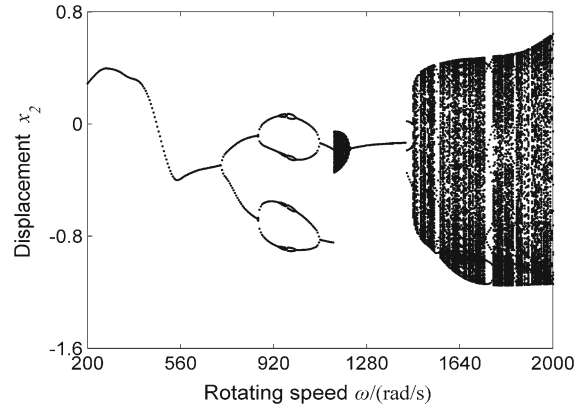

Fig. 8 Bifurcation diagram at $A = 0.5$, $k_c = 3.5 \times 10^6\,\text{N m}^{-1}$

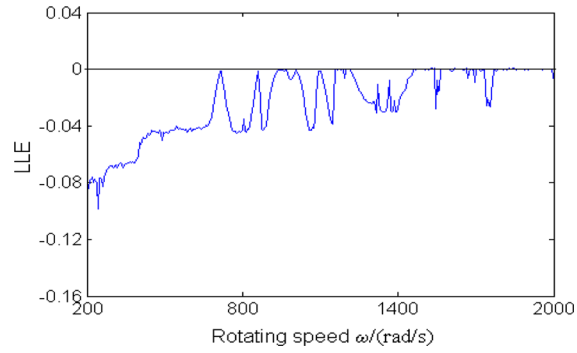

Fig. 9 Largest Lyapunov exponent at $A = 0.5$, $k_c = 3.5 \times 10^6\,\text{N m}^{-1}$

3.2 Effect of crack depth to the system

Figure 8 shows the bifurcation diagram, and Fig. 9 represents the LLE at a higher crack depth ($A = 0.5$) in comparison with Fig. 3 ($A = 0$). In this case, the responses of the system exhibit similar dynamic phenomena. It is found that the system works in P1 motion (see Fig. 10) until the first bifurcation happens at $\omega = 715\,\text{rad/s}$, which appears later compared with Fig. 3 ($A = 0$). From Figs. 8 and 9, it can be seen that the system takes a series of motions {P2 $\rightarrow$ P4 $\rightarrow$ P8 $\rightarrow$ P8 $\rightarrow$ P4 $\rightarrow$ P2} at $\omega = [715-1140]\,\text{rad/s}$. Although oil whirl and rub-impact have influences on the system, the existence of crack has weakened the fault level (see Fig. 11). The system begins the long-term quasiperiodic motion from $\omega = 1460\,\text{rad/s}$ (see Fig. 8). Time series, axis orbit, frequency spectra and Poincare map at $\omega = 1550\,\text{rad/s}$ are shown in Fig. 12. It can be seen that partial quasiperiodic window evolves into some multi-periodic windows after the oil-whip occurs.

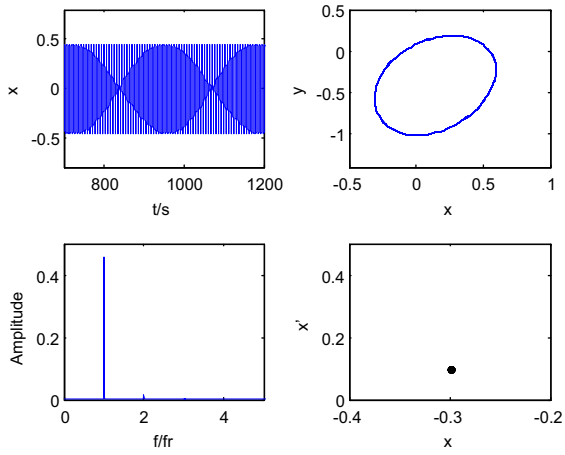

Fig. 10 Time series, axis orbit, frequency spectra and Poincare map at $\omega = 705\,\text{rad/s}$

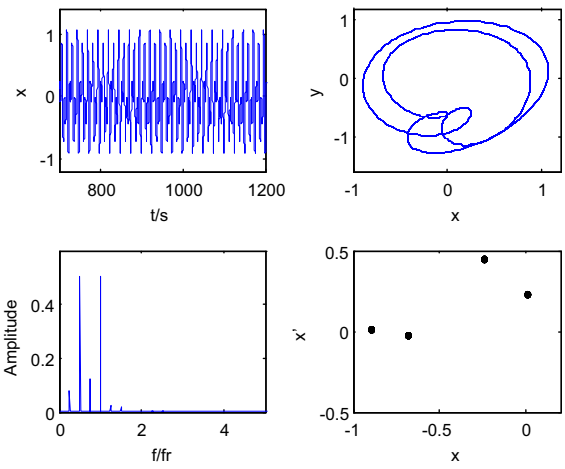

Fig. 11 Time series, axis orbit, frequency spectra and Poincare map at $\omega = 1050\,\text{rad/s}$

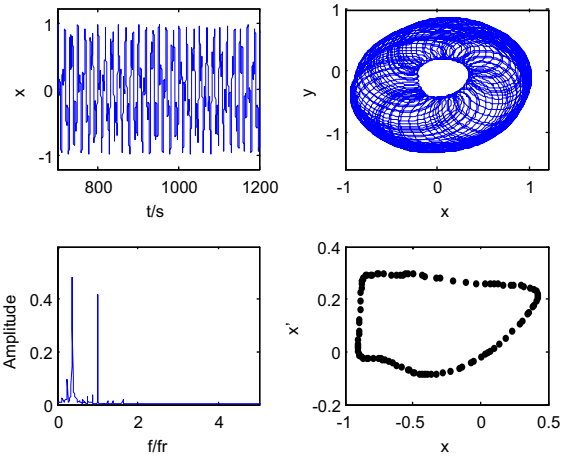

Fig. 12 Time series, axis orbit, frequency spectra and Poincare map at $\omega = 1550\,\text{rad/s}$

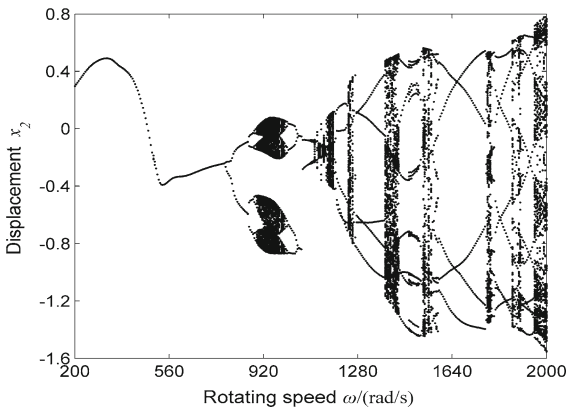

Fig. 13 Bifurcation diagram at $A = 0.9$, $k_c = 3.5 \times 10^6\,\text{N m}^{-1}$

It can also be found in Fig. 9 that the values of the LLE proceed to the change {negative number $\rightarrow 0 \rightarrow$ negative number $\rightarrow 0 \rightarrow$ negative number $\rightarrow 0$}. The result illustrates that the crack can enhance the nonlinearity of the system in the region high rotating speed.

Figure 13 shows the bifurcation diagram, and Fig. 14 represents the LLE at a higher crack depth ($A = 0.9$). In this case, the responses of the system exhibit complex nonlinear phenomena. It is found that the system works in P1 motion (see Fig. 10) until the first bifurcation happens at $\omega = 770\,\text{rad/s}$, which appears later compared with Fig. 3 ($A = 0$) and Fig. 8 ($A = 0.5$). It can be seen from the results that the instability speed of the system increases as the crack depth growing. This lagged bifurcation indicates that the crack interferes with the formation of oil whirl and there exists the interaction between faults. This is the same as the results obtained from the Ref. [20]. However, this phenomenon does not mean the increase of crack depth is benefit for the system. When the crack depth hits a certain level, a serious accident may happen. Then, after several period-doubling bifurcations because of the oil-film force, the system runs into chaos (see Fig. 15), whose LLE is greater than zero. As the rotational speed increases, the unbalance force becomes the main factor affecting the system, thus, making the system exit chaos and go back to the periodic motion. In the high speed area, the long-term quasiperiodic motion turns into intermittent chaos where the multi-periodic motion and chaos

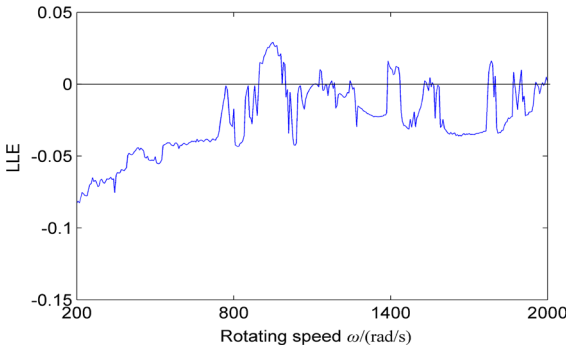

Fig. 14 Largest Lyapunov exponent at $A = 0.9, k_c = 3.5 \times 10^6\,\mathrm{N\,m^{-1}}$

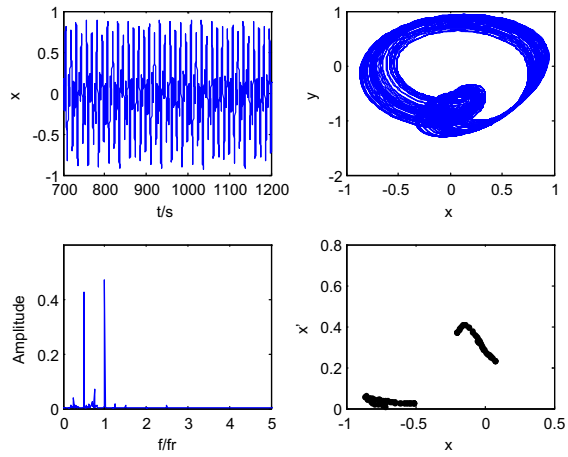

Fig. 15 Time series, axis orbit, frequency spectra and Poincare map at $\omega = 960\,\mathrm{rad/s}$

appear alternately (see Figs. 16, 17). It also can be seen from Fig. 14 that the value of the LLE has more fluctuation. This indicates the crack depth has more impacts on the response of the system in high speed area. The crack strengthens the oil whip and rub-impact faults, and the system takes on strong nonlinearity and instability.

3.3 Effect of stator stiffness to the system

The stator stiffness, which is in proportion to rub-impact force of the rotor system shown in Eq. (5), plays a significant role in dynamic analysis of rotor system. Bifurcation diagram for stator stiffness parameter $k_c = 7 \times 10^6\,\mathrm{N\,m^{-1}}$ is shown in Fig. 18. The largest Lyapunov exponent for this parameter of the system is shown in Fig. 19. From Fig. 18, it

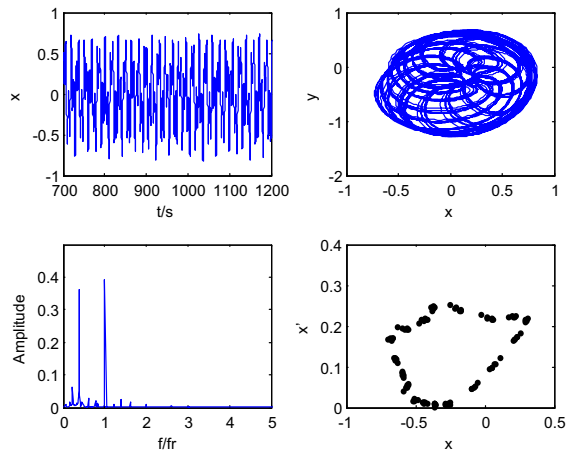

Fig. 16 Time series, axis orbit, frequency spectra and Poincare map at $\omega = 1245\,\mathrm{rad/s}$

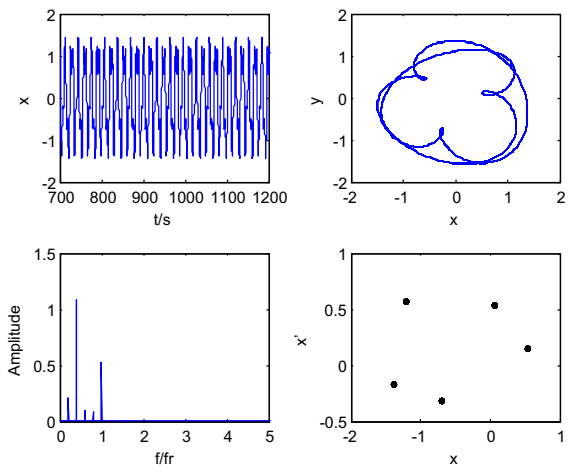

Fig. 17 Time series, axis orbit, frequency spectra and Poincare map at $\omega = 1760\,\mathrm{rad/s}$

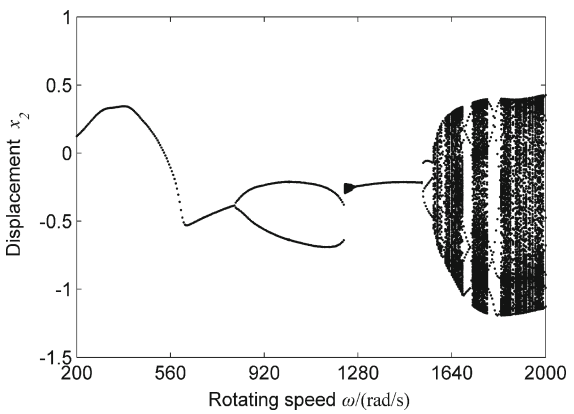

Fig. 18 Bifurcation diagram at $A = 0.5, k_c = 7 \times 10^6\,\mathrm{N\,m^{-1}}$

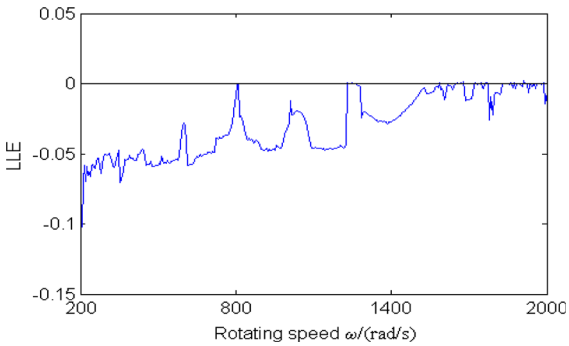

Fig. 19 Largest Lyapunov exponent at $A = 0.5, k_c = 7 \times 10^6\,\mathrm{N\,m^{-1}}$

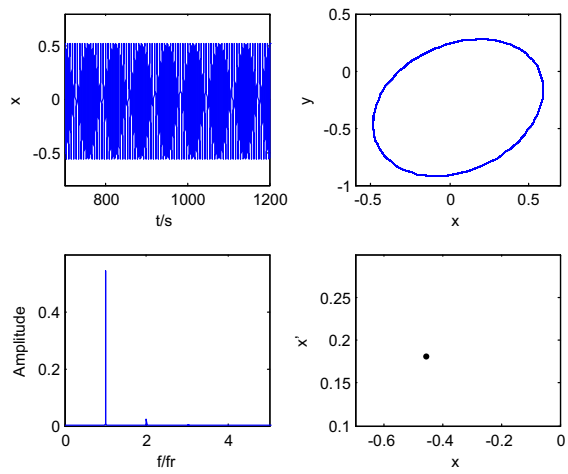

Fig. 20 Time series, axis orbit, frequency spectra and Poincare map at $\omega = 705\,\mathrm{rad/s}$

can be seen that the system goes through dynamic motions {P1 → P2 → quasiperiodic motion → P1 → intermittent quasiperiodic motion}. Compared with Fig. 8 ($k_c = 3.5 \times 10^6\,\mathrm{N\,m^{-1}}$), bifurcation times in this situation decreases, and the first bifurcation point occurs at $\omega = 805\,\mathrm{rad/s}$, which lags the first bifurcation point in Fig. 8. The system is in a steady state before this speed (see Fig. 20). When the rotating speed gets higher values than 1530 rad/s, several multi-periodic motions appear among the long-term quasi-periodic motion, which also can be observed in Fig. 19. And the oil-film instability and rub-impact exist at the same time and become aggravating as speed increases (see Figs. 21, 22).

To further study the dynamical influence of the stator stiffness on this coupled system, the stator stiffness is added to $k_c = 1.8 \times 10^7\,\mathrm{N\,m^{-1}}$. Bifurcation

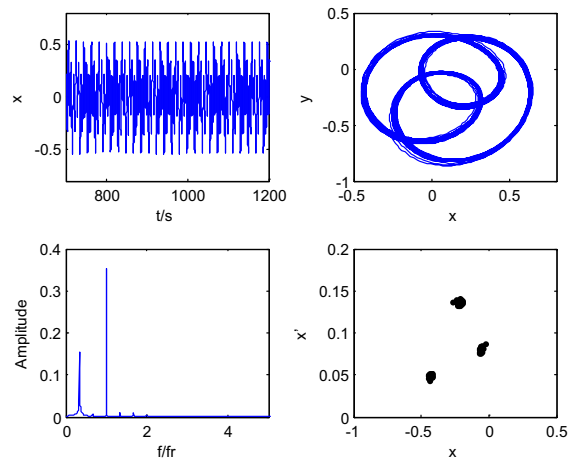

Fig. 21 Time series, axis orbit, frequency spectra and Poincare map at $\omega = 1550\,\mathrm{rad/s}$

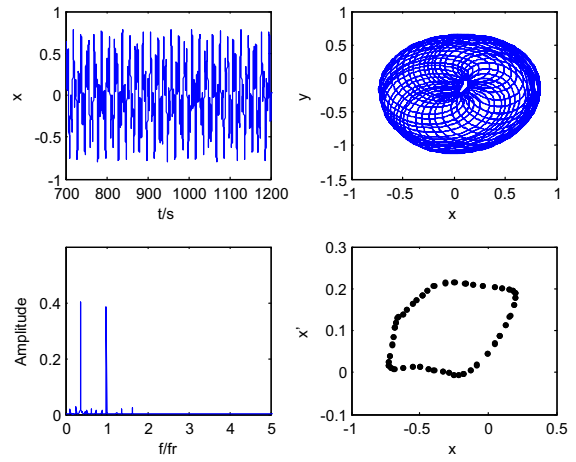

Fig. 22 Time series, axis orbit, frequency spectra and Poincare map at $\omega = 1595\,\mathrm{rad/s}$

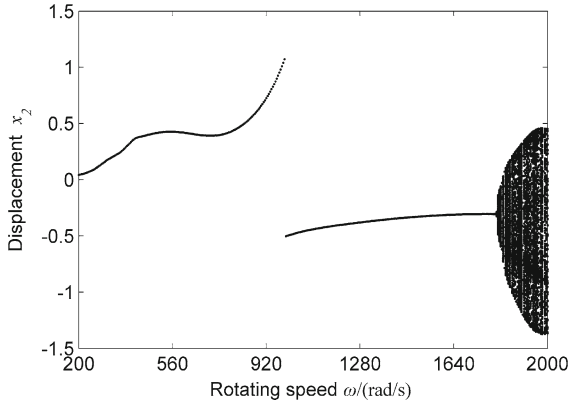

Fig. 23 Bifurcation diagram at $A = 0.5, k_c = 1.8 \times 10^7\,\mathrm{N\,m^{-1}}$

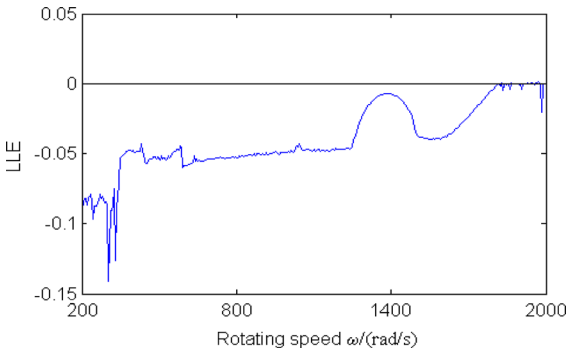

Fig. 24 Largest Lyapunov exponent at $A = 0.5, k_c = 1.8 \times 10^7\,\mathrm{N\,m^{-1}}$

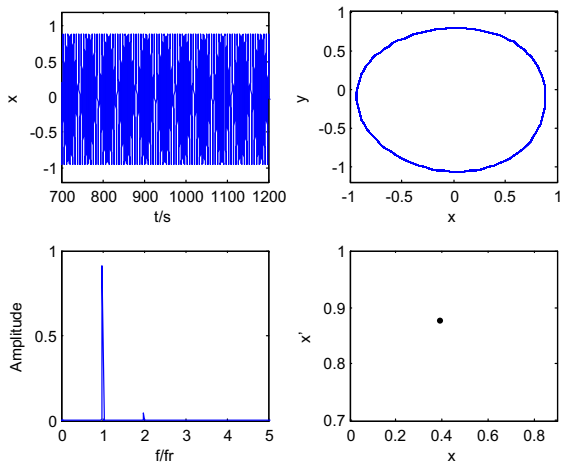

Fig. 25 Time series, axis orbit, frequency spectra and Poincare map at $\omega = 705\,\mathrm{rad/s}$

diagram for this parameter of the system is shown in Fig. 23, and the largest Lyapunov exponent is shown in Fig. 24. Compared with Fig. 18 ($k_c = 7 \times 10^6\,\mathrm{N\,m^{-1}}$), the dynamic behavior of the system at $k_c = 1.8 \times 10^7\,\mathrm{N\,m^{-1}}$ gets much simpler. This means increasing the stator stiffness value can enhance the stability of the system. The motions of the system go through a process {P1 $\rightarrow$ quasiperiodic motion}. The oil whirl motion does not occur. In Figs. 23 and 24, it is obvious that the system works in the stable P1 motion from $\omega = 200\,\mathrm{rad/s}$ to $1810\,\mathrm{rad/s}$ (see Fig. 25). The quasiperiodic motion comes out at $\omega = 1815\,\mathrm{rad/s}$. Time series, axis orbit, frequency spectra and Poincare map at $\omega = 1830\,\mathrm{rad/s}$ and $\omega = 1950\,\mathrm{rad/s}$ are shown in Figs. 26 and 27, respectively. The two motions of the system are the quasiperiodic motion.

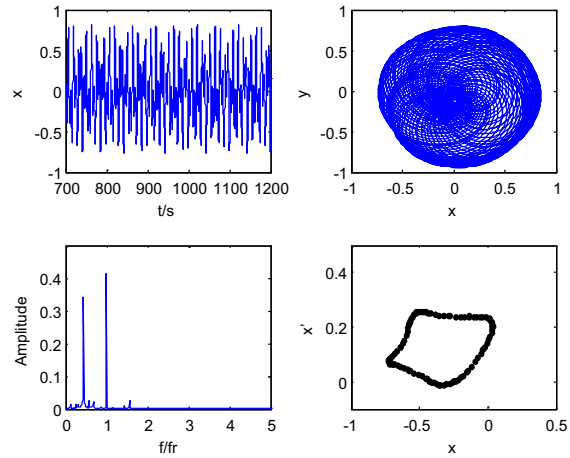

Fig. 26 Time series, axis orbit, frequency spectra and Poincare map at $\omega = 1830\,\mathrm{rad/s}$

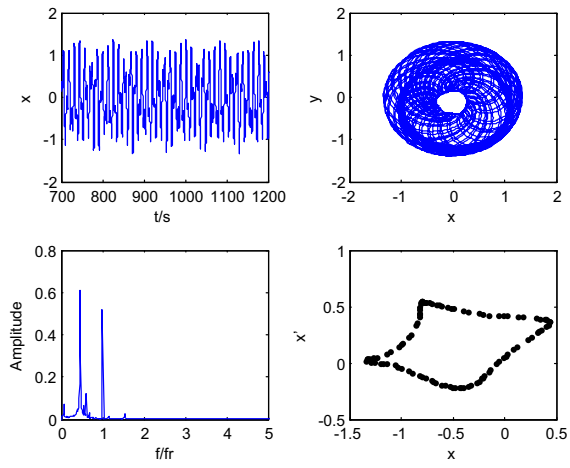

Fig. 27 Time series, axis orbit, frequency spectra and Poincare map at $\omega = 1950\,\mathrm{rad/s}$

4 Conclusion

A nonlinear model is built to study dynamic behaviors of the single disk rotor-bearing system with interaction among crack, rub-impact and oil-film force. This modeling strategy has adopted the time-varying stiffness model to simulate the stiffness of a crack rotor and employed the short bearing theory to describe the oil-film force. The numerical simulation results reveal that this system exists rich nonlinear phenomena, such as the period-doubling bifurcation, the multi-period and the quasiperiodic motions. The comparisons of the dynamic behaviors of different parameters indicate that

crack depth and stator stiffness influence the vibration and instability of the system with varied rotating speed. In summary, the system has strong nonlinearity and instability in high speed region. Moreover, crack depth and stator stiffness can interfere with the formation of oil whirl, thus, making the oil whirl appear later. The results demonstrate that the stability of the system is affected by the system parameters, and there exists interaction among all fault forces. We have conducted experiments on the rotor-bearing system with rub-impact and oil-film instability [22]. And the conclusion about the effect of stator stiffness on the system is consistent with the results from experiments. Next we will employ the experiment on the test rig to study the effects of various parameters on the response of the system and verify the numerical results.

Acknowledgments This work is supported by the National Natural Science Foundation of China (No. 51475164) and Natural Science Foundation of Hebei Province (E2013502226).

References

1. Dimarogonas, A.D.: Vibration of cracked structures: a state of art review. Eng. Fract. Mech. **55**, 831–857 (1996)
2. Gash, R.: A survey of the dynamic behavior of a simple rotating shaft with a transverse crack. J. Sound Vib. **160**, 313–332 (1993)
3. Jun, O.S., Eun, H.J., Earmme, Y.Y., Lee, C.W.: Modelling and vibration analysis of a simple rotor with breathing crack. J. Sound Vib. **155**, 273–290 (1992)
4. Sekhar, A.S., Prabhu, B.S.: Transient analysis of a cracked rotor passing through critical speed. J. Sound Vib. **173**, 415–421 (1994)
5. Sinou, J.J., Lees, A.W.: The influence of cracks in rotating shafts. J. Sound Vib. **285**, 1015–1037 (2005)
6. Chan, R.K., Lai, T.C.: Digital simulation of a rotating shaft with a transverse crack. Appl. Math. Model. **19**, 411–420 (1995)
7. Darpe, A.K., Gupta, K., Chawla, A.: Dynamics of a two-cracked rotor. J. Sound Vib. **259**, 649–675 (2003)
8. Darpe, A.K., Gupta, K., Chawla, A.: Dynamics of a bowed rotor with a transverse surface crack. J. Sound Vib. **296**, 888–90 (2006)
9. Guang, M.: The nonlinear influences of whirl speed on the stability and response of a cracked rotor. J. Mach. Vib. **6**, 216–230 (1992)
10. Gounaris, G.D., Papadopoulos, C.A.: Crack identification in rotating shafts by coupled response measurements. Eng. Fract. Mech. **69**, 339–352 (2002)
11. Muszynska, A.: Rotor-to-stationary element rub-related vibration phenomena in rotating machinery literature survey. Shock Vib. Dig. **21**, 3–11 (1989)
12. Chu, F., Zhang, Z.: Bifurcation and chaos in rub-impact Jeffcott rotor system. J. Sound Vib. **210**, 1–18 (1998)
13. Goldman, P., Muszynska, A.: Chaotic behavior of rotor/stator systems with rubs. J. Eng. Gas Turbines Power **116**, 692–701 (1994)
14. Abu-Mahfouz, Issam, Banerjee, Amit: On the investigation of nonlinear dynamics of a rotor with rub-impact using numerical analysis and evolutionary algorithms. Procedia Comput. Sci. **20**, 140–147 (2013)
15. Liu, L., Cao, D.Q., Sun, S.P.: Dynamic characteristics of a disk-drum-shaft rotor system with rub-impact. Nonlinear Dyn. **80**, 1017–1038 (2015)
16. Lahriri, S., Santos, I.F.: Theoretical modelling, analysis and validation of the shaft motion and dynamic forces during rotor–stator contact. J. Sound Vib. **332**, 6359–6376 (2013)
17. Chang-Jian, C.-W., Chen, C.-K.: Couple stress fluid improve rub-impact rotor-bearing system—nonlinear dynamic analysis. Appl. Math. Model. **34**, 1763–1778 (2010)
18. Shen, X.Y., Jia, J.H., Zhao, M.: Experimental and numerical analysis of nonlinear dynamics of rotor-bearing-seal system. Nonlinear Dyn. **53**, 31–44 (1996)
19. Wan, F., Xu, Q., Li, S.: Vibration analysis of cracked rotor sliding bearing system with rotor–stator rubbing by harmonic wavelet transform. J. Sound Vib. **271**, 507–518 (2004)
20. Ren, Z., Zhou, S., Li, C., Wen, B.: Dynamic characteristics of multi-degrees of freedom system rotor-bearing system with coupling faults of rub-impact and crack. Chin. J. Mech. Eng. **27**, 785–792 (2014)
21. Adiletta, G., Guido, A.R., Rossi, C.: Chaotic motions of a rigid rotor in short journal bearings. Nonlinear Dyn. **10**, 251–269 (1996)
22. Aijun, Hu, Yan, Xiaoan, Xiang, Ling: Dynamic simulation and experimental study of an asymmetric double-disc rotor-bearing system with rub-impact and oil-film instability. Nonlinear Dyn. **84**, 641–659 (2016)